

Frequency Dependent Rays of qP-Waves in 3D Weak Tilted Transversely Isotropic (TTI) Media

Dmitry Neklyudov(✉) and Maxim Protasov

Institute of Petroleum Geology and Geophysics SB RAS, Prospect Acad. Koptuga 3, 630090 Novosibirsk, Russia
neklyudovda@ipgg.sbras.ru

Abstract. The paper provides a simple and numerically effective method to calculate frequency dependent rays of qP-wave in three-dimensional TTI media. Our method involves propagating a locally plane fragment of the wave front, which is sensitive to the distribution of the model parameters in some sub volume of the medium near a ray. The wavelength in each point on the ray determines the width of the sensitivity area. For numerical realization we apply approximate expressions for phase and group velocities which are valid for weak TTI media. Numerical experiments demonstrate the effectiveness of the proposed approach.

Keywords: Frequency dependent rays · anisotropy · TTI

1 Introduction

The ray method [1, 2] plays an important role in seismic data processing. The implementation of key seismic data processing procedures, such as seismic travel-time tomography and Kirchhoff migration are based on the ray tracing. First, the ray method is used to calculate ray trajectories and the first arrival travel-times of seismic waves. The classical formulation of the ray method relies on high-frequency approximations to obtain solutions to the system of equations in the dynamic theory of elasticity. The use of such approximation neglects the fact that real seismic signals are broad-band and have limited spectra. Because of such approximation, rays exhibit "unphysical" behavior in models with significant inhomogeneities and sharp interfaces [3, 4]. The rays in these circumstances become unpredictable and differ significantly from the expected propagation path. Shadow zones, which are areas where rays cannot pass, are present in the computational domain. Firstly, this behavior clearly contradicts the physics of real seismic wave propagation processes. In complex geological environments, ray based seismic data processing procedures such as tomography may produce inaccurate results [5]. It is necessary to overcome the limitations of the standard ray method in practice. It is known that the distribution of physical parameters influences the propagation of a signal with a limited band-width inside a specific volume located in the vicinity of a ray [6, 7]. This volume is referred to as the "Fresnel volume". The dominant frequency of the signal determines its width. Quite some time ago, researchers realized that they

© The Author(s), under exclusive license to Springer Nature Switzerland AG 2024
O. Gervasi et al. (Eds.): ICCSA 2024, LNCS 14813, pp. 268–282, 2024.
https://doi.org/10.1007/978-3-031-64605-8_19

needed to consider this fact and reduce the limitations of the ray method associated with high-frequency approximation. Several approaches have been proposed [8–13] to solve this problem, with varying degrees of effectiveness. All of these approaches have their advantages and disadvantages. The most significant drawback is the computational complexity, which becomes particularly apparent when considering the three-dimensional case. The paper [9] presented a promising approach that approximates the propagation of broadband seismic signals through frequency dependent ray tracing. The key finding is that the velocity used for ray tracing is determined by smoothing actual velocity along a locally flat element of the wave front. The aperture of such smoothing is chosen proportional to the wavelength. A predefined parameter, which has a frequency dimension controls the wavelength. Compared to the standard ray method, the differential equations that describe ray propagation are almost unchanged, except for substituting interval velocities with velocities smoothed along the wave front. In [14], an adaptation of this idea without solving a system of differential equations was proposed. The method is designed for the calculation of frequency-dependent rays in 3D acoustic media. The ray tracing procedure involves moving a locally flat fragment of a wave front whose orientation depends on the velocity distribution inside a certain frequency-dependent aperture. The parameters of the medium affect the ray within a certain volume around it. We refer to it as a "fat" ray because of this reason. The suggested approach has proven to be robust and easy to implement. Numerical experiments demonstrate that "fat" rays are more stable in complex situations than standard rays, and may provide reliable traveltimes and trajectories when the standard ray method fails.

The industry widely acknowledges the need to consider seismic anisotropy in data processing practices. This paper discusses an algorithm that can be used to compute frequency-dependent rays of qP-waves (quasi-primary waves) in a three-dimensional tilted transversely isotropic (TTI) medium with arbitrary oriented symmetry axis. It is an extension of the approach proposed in [14] for anisotropy. Numerical experiments prove that "fat" rays can be quite successfully used for rays and travel-times calculation in complex three-dimensional TTI media.

2 Approximate Expressions for Phase and Group Velocities of qP-Waves in Weak TTI Media

The following section presents approximate expressions for the phase and group velocities of qP-waves that we used to calculate frequency dependent rays in weak TTI media.

In most realistic cases, the assumption of weak anisotropy is fulfilled [15]. By making this assumption, the expressions for phase and group velocities can be greatly simplified, which significantly increases the computational efficiency of ray tracing in anisotropic media [16, 17]. The weak anisotropy assumption means that the stiffness tensor of anisotropic medium c_{ijkl} can be decomposed into two components $c_{ijkl} = c^{ISO}_{ijkl} + \delta c_{ijkl}$, where c^{ISO}_{ijkl} is the reference isotropic component of the model, δc_{ijkl} is anisotropic component which is small compared to reference isotropic term. Practical experience demonstrates that the weak anisotropy assumption is valid if the anisotropic term is no more than 10% of the isotropic reference value.

Consider Christoffel matrix whose elements depend on the direction vector $\overrightarrow{p}$, $\Gamma_{jk} = p_i p_l a_{ijkl}$, where $a_{ijkl} = c_{ijkl}/\rho$ are density normalized stiffness tensor elements, p_j are components of the slowness vector $\overrightarrow{p}$ which is related to the phase velocity V in the normal direction to the wave front, $\overrightarrow{p} = \overrightarrow{n}/V(\overrightarrow{n})$. Vector $\overrightarrow{n}$ is a unit normal vector to the front. Three types of waves can exist in an arbitrary anisotropic medium: qP, qSV, qSH. Each wave mode corresponds to one of the three eigenvalues of the Christoffel matrix. qP-wave corresponds to the largest eigenvalue. Its wave polarization vector coincides with the first eigenvector. The phase velocity is determined by the eigenvalue of the Christoffel matrix $G(\overrightarrow{n})$ as:

$$V^2\left(\overrightarrow{n}\right) = G(\overrightarrow{n}) \tag{1}$$

The group velocity components are given by the expression:

$$v_j = \frac{1}{2}\frac{\partial G(\overrightarrow{p})}{\partial p_j} \tag{2}$$

In seismic exploration, the propagation of qP-waves is mostly interesting. A set of parameters that has become standard for most practical applications is used to parametrize the anisotropic medium, when only qP-waves are taken into account [18]: V_p is the phase velocity of qP-waves along the symmetry axis, two angles characterizing orientation of symmetry axis in each point, θ_{AZ} (azimuth) and θ_{DIP} (dip angle regarding to vertical axis) and two anisotropy parameters, ε, δ (so called Thomsen parameters), [15]. The Thomsen parameters are expressed through the density-normalized stiffness tensor coefficients in the following manner: $\varepsilon = \frac{a_{11}-a_{33}}{2a_{33}}$, $\delta = \frac{a_{13}-a_{33}+2a_{44}}{a_{33}}$. [19] presented a simplified way to calculate the qP-wave eigenvalue in vertical transversely isotropic (VTI) media (vertical symmetry axis), under the assumption of weak anisotropy. In the paper [20], a generalization of this expression is provided for a tilted transversely isotropic medium with an arbitrary orientation of the symmetry axis.

Let $\overrightarrow{e}$ be a unit vector that defines the orientation of the symmetry axis. $\overrightarrow{e}$ is parallel to the axis of symmetry. Its components are expressed via angles θ_{AZ}, θ_{DIP} as $\overrightarrow{e} = (sin\theta_{DIP} \cdot cos\theta_{AZ}, sin\theta_{DIP} \cdot sin\theta_{AZ}, cos\theta_{DIP})$. We make use of the following notations below: $P = \left|\overrightarrow{p}\right|^2$ is the square of the norm of the slowness vector, $D = \overrightarrow{e} \cdot \overrightarrow{p}$ is the dot product of the vectors $\overrightarrow{e}$ and $\overrightarrow{p}$, $D_N = \overrightarrow{e} \cdot \overrightarrow{n}$ is the dot product of the unit normal $\overrightarrow{n}$ and the vector $\overrightarrow{e}$. Using these notations, it is possible to write an approximate expression for the first eigenvalue of the Christoffel matrix [20]:

$$G(\vec{x}, \vec{p}) = V_P^2\{P(1+2\varepsilon) + 2(\delta - 2\varepsilon)D^2 - 2(\delta - \varepsilon)\frac{D^4}{P}\}. \tag{3}$$

Phase velocity of qP-wave in the direction normal to the front is defined by the expressions (1) and (3):

$$V^2(\vec{x}, \vec{n}) = V_P^2\{1 + 2\varepsilon + 2(\delta - 2\varepsilon)D_N^2 - 2(\delta - \varepsilon)D_N^4\}, \tag{4}$$

Regarding the formula (2), by calculating derivatives of the eigenvalue $G\left(\overrightarrow{x}, \overrightarrow{p}\right)$ with respect to the components of the slowness vector $\overrightarrow{p}$, the approximate expression

for the components of the group (ray) velocity $\overrightarrow{v}$ is found:

$$v_j = \frac{1}{2}V_P^2\left\{\left[2(1+2\varepsilon)+4(\delta-\varepsilon)\frac{D^4}{P^2}\right]p_j+\left[2(\delta-2\varepsilon)D-8(\delta-\varepsilon)\frac{D^3}{P}\right]e_j\right\}, \quad (5)$$

where p_j and e_j are components of the vectors $\overrightarrow{p}$ и $\overrightarrow{e}$ respectively. The value of the group velocity is given as $v = |\overrightarrow{v}|$.

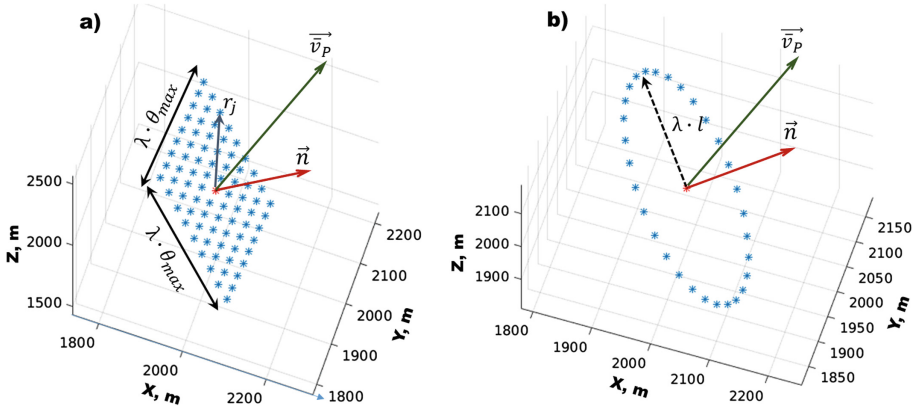


Fig. 1. a) Rectangular area cut along a locally flat wave front. The blue asterisks represent the points in the regular grid where phase velocity values are calculated for smoothing along the wave front. The central point is shown as a red star. Vector $\overrightarrow{n}$ denote current normal to the front. Green arrow shows group velocity vector (ray propagation direction). b) The control points are situated around the central point on the ray in the plane of the wave front. They are employed to determine the normal to the front during the next step along the ray. (Color figure online)

3 "Fat" Ray in 3D TTI Media

In [14], we proposed an algorithm for the calculation of frequency dependent rays ("fat" rays) in three-dimensional acoustic media. Below, we describe the adaptation of this method to weak TTI media. The basic idea inherent in "fat" rays is to take into account the distribution of physical parameters of the medium in the vicinity of a ray. The predetermined parameter, which has a frequency dimension, controls the width of this area. By decreasing the frequency (i.e. by increasing the wavelength), a "fat" ray can be made "wider", i.e. more sensitive to the parameters of the model or vice versa, to obtain "fat" rays that are similar to the ones provided by the classical ray method. A fragment of a locally flat wave front is propagated when tracing the "fat" ray. For each moment of time, "fat" ray tracing procedure consists of two stages. In the first stage, the ray moves from the known position towards a known direction that is determined by the current orientation of the unit wave front normal (in the isotropic case, direction of ray movement coincides with the normal to the front). Smoothed model parameters are used to make an elementary step along the ray. Smoothing is performed along a locally

flat wave front element centered on the ray. As a result of this stage, the ray position is determined at the next moment of time. The second stage involves determining the orientation of the locally flat wave front at the new point on the ray. The movement of a set of 'control' points that are specifically chosen near the ray in the plane of the wave front is used for this purpose. The wavelength at the point on the ray determines how far the control points are located from the ray. The wavelength governs the sensitivity of the ray. Next, we describe how these steps are performed with the TTI media.

As an input to the procedure, two take-off angles φ_{AZ}, φ_{Dip} are given which define initial orientation of the wave front normal, where φ_{AZ} is azimuthal angle (an angle between initial normal direction and lateral X-axis in XY plane), φ_{Dip} is dip angle (an angle between initial normal and vertical (Z) coordinate axis). Also we define auxiliary parameter υ measured in Hz, which is called "frequency" of the ray.

1) Let $\overrightarrow{x}_p = (x_p, y_p, z_p)$ is a current point on the ray (we will call it the central point further). A unit vector $\overrightarrow{n} = (n_X, n_Y, n_Z)$ is given at this point that defines a normal to the front. To begin with, let's explain how the model parameters are smoothed in the vicinity of the ray along the flat wave front element. We construct a plane passes through the point $\overrightarrow{x}_p$ and orthogonal to the vector $\overrightarrow{n}$. A rectangle is cut with the center at point $\overrightarrow{x}_p$ in this plane, which has sizes that are dependent on the wavelength $\lambda = \frac{V(\overrightarrow{x}_p, \overrightarrow{n})}{\upsilon}$ as it is shown in Fig. 1a, where $V(\overrightarrow{x}_p, \overrightarrow{n})$ is the phase velocity in the point $\overrightarrow{x}_p$, υ is the frequency. A regular grid is defined on the selected wave front fragment. In Fig. 1a, blue asterisks represent these grid points. The phase velocity values $V(\overrightarrow{x}_j, \overrightarrow{n})$ at every point of the grid are determined by formula (4) using the same normal to the front $\overrightarrow{n}$. At the central point, the weighted sum of all phase velocities is used to calculate the value of the smoothed phase velocity along the flat wave front element:

$$V_{sm}\left(\overrightarrow{x}_p, \overrightarrow{n}, v\right) = \frac{\sum_{j=-N}^{N} w_j \cdot V(\overrightarrow{x}_j, \overrightarrow{n})}{\sum_{j=-N}^{N} w_j} \tag{6}$$

where w_j are the smoothing weights, N is a total number of grid points. 2D Gaussian function is used as a smoother. Here, the weights are given as:

$$w_j = \exp\left\{-\left(\frac{r_j}{\lambda \cdot \theta_{max} \cdot \alpha}\right)^2\right\} \tag{7}$$

where r_j is a distance between the central point and the point $\overrightarrow{x}_j$ in the wave front rectangular element. The input parameter θ_{max} defines which part of the wavelength is taken into account when choosing the smoothing aperture. Parameter α is responsible for the shape of Gaussian smoother [14]. When the parameter α is reduced, the smoothing function becomes narrower, concentrating near the center point. When increasing the parameter α, the Gaussian smoothing is reduced to simple averaging in the rectangular area.

Let dt be the time step along the ray. To move along the ray, the following scheme is applied (see Fig. 2). At the center point $\overrightarrow{x}_p$, the value of the smoothed phase velocity $\overline{V}_p = V_{sm}(\overrightarrow{x}_p, \overrightarrow{n}, v)$ is calculated as described above. Using the phase velocity $\overline{V}_p$ and

the normal to the front $\vec{n}$, the corresponding group velocity vector $\vec{v}_P(\vec{n}) = (v_x, v_y, v_z)$ are calculated using the expression (5). During the time interval dt, the central point $\vec{x}_p$ moves to the certain new point $\vec{x}_p + d\vec{x}_p$ along the group velocity vector, where $d\vec{x}_p = (dx_p, dy_p, dz_p)$:

$$dx_p = dt \cdot v_x, dy_p = dt \cdot v_y, dz_p = dt \cdot v_z \tag{8}$$

It gives us a position of a next point on the ray. Now we need to determine wave front orientation at this point.

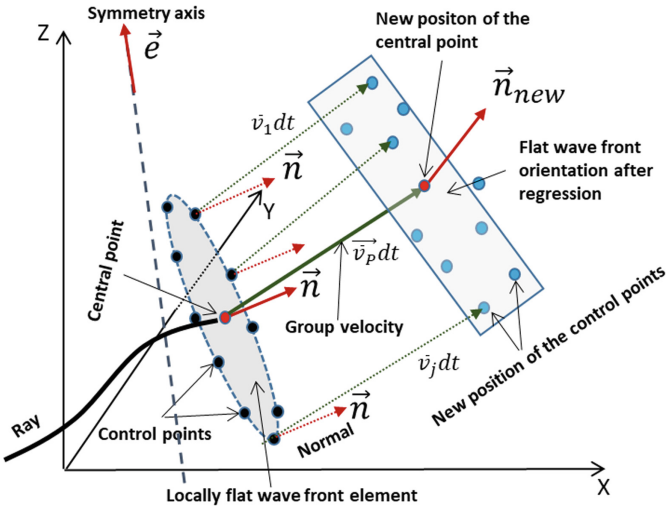


Fig. 2. Scheme of "fat" ray tracing in TTI medium (see the text for more details).

2) We do the following to establish the orientation of the wave front at the new point on the ray. Consider a circle lying within the plane of the wave front. The radius of the circle also depends on the local wavelength,R $= \lambda \cdot l$, where the parameter l has the same meaning as the parameterθ_{max}, controls the smoothing aperture width, but it is not necessary to have the same value. We pick a set of points on the circle that have constant angles increment (see Fig. 1b). Further, these points are referred to as "control" points. For each control point located on a circle centered on the ray, a group velocity vector $\vec{v}_j(\vec{x}_j, \vec{n}) = (v_x^j, v_y^j, v_z^j)$ is calculated using the given normal to the wave front $\vec{n}$ by expression (5). For the same time interval,dt, the control points will travel different distances because group velocity values may differ: $dx_j = dt \cdot v_x^j, dy_j = dt \cdot v_y^j$, $dz_j = dt \cdot v_z^j$. It's highly probable that the new control points locations $\vec{x}_j + d\vec{x}_j$ won't be on the same plane. In order to determine the new orientation of the locally flat wave front, we calculate the plane that is closest to all points $\vec{x}_j + d\vec{x}_j$ in the least-squares sense. As a result, the classical linear regression problem arises. The numerical solution of the problem allows us to determine a new normal vector to the front, $\vec{n}_{new}$. We attach $\vec{n}_{new}$ to the new central point position $\vec{x}_p + d\vec{x}_p$ and repeat the process. Thus, there is

a step-by-step movement along the ray. When the scheme is implemented, a locally flat fragment of the wave front moves. The physical parameters of the model in a particular vicinity of the ray affect its orientation at each moment of time.

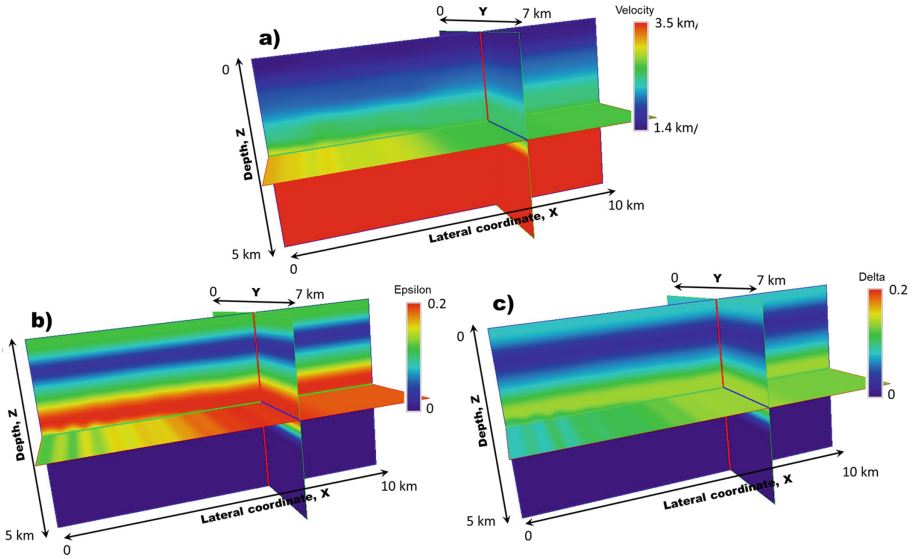


Fig. 3. Realistic 2.5D VTI model. a) Phase velocity along the vertical symmetry axis, b) Dimensionless Thomsen parameter ε distribution (its variations are within the interval [0 - 0.2]), c) Dimensionless Thomsen parameter δ distribution (its variations are within the interval [0 - 0.14]).

4 Numerical Examples

4.1 Numerical Verification: Comparison of "Fat" Rays with Standard Rays in a Smooth VTI Model

We verify the effectiveness of the proposed approach by comparing the frequency dependent rays constructed according to the proposed scheme with the standard rays in the smooth model. We choose the smooth model to prevent problems during the calculation of standard rays, as they exhibit unpredictable behavior when there are sharp inhomogeneities within the model. As the theory predicts, if the "ray frequency" parameter υ increases, the "fat" rays tend to be closer to the standard rays [9, 14]. Fat rays and standard rays become identical when the parameter υ reaches a certain value (as it was demonstrated by numerical experiments for the acoustic case, $\upsilon > 30$ Hz). The numerical validation of the proposed scheme will be based on this fact.

The numerical experiments presented below are based on a realistic model obtained during real seismic data processing. Dataset was acquired in some oil production area in Eastern Siberia. Anisotropic reflection travel-time tomography was utilized to recover

model parameters [21]. The model depicted in Fig. 3 is only dependent on two coordinates (X and Z). In order to obtain a three-dimensional model, two-dimensional sections of phase velocity distribution and Thomsen parameters ε, δ, recovered along one profile, were "replicated" in the cross-line direction (along lateral Y axis). Symmetry axis is vertical at each point of the model (VTI model).

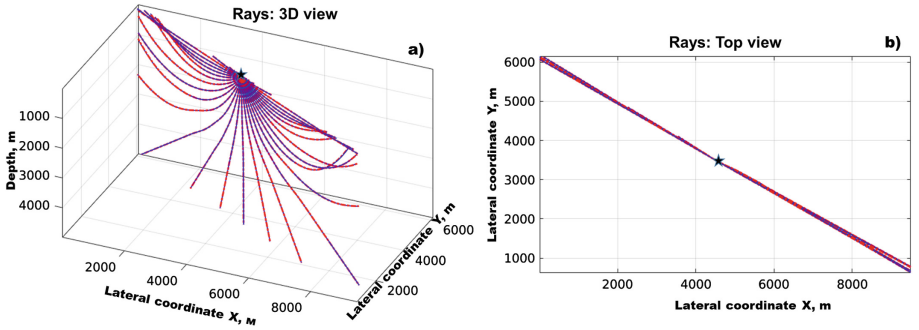


Fig. 4. Comparison of rays calculated in the VTI model from Fig. 3 for one source location (marked as asterisk) and one fixed azimuth $\varphi_{AZ} = -30°$: a) 3D view of rays, b) rays projection at XY plane (top view). "Fat" rays calculated for frequency parameter $\upsilon = 30$ Hz are shown in blue, standard rays are shown in red. (Color figure online)

The phase velocities of the qP-waves along the vertical axis of symmetry vary between 1400 and 3500 m/s. The dimensionless Thomsen parameters ε and δ lie within ranges of [0–0.2] and [0–0.14] respectively. The model is provided on a regular grid with the same spatial step in all directions, $dx = dy = dz = 10$ m, number of grid points are $N_X = 951, N_Y = 701, N_Z = 501$. Total spatial size of the model is 9500 x 7000 x 5000 m (two lateral directions and depth respectively). For "fat" ray construction the following parameters have been used: "ray frequency" $\upsilon = 30$ Hz, $l = 0.25$, $\theta_{max} = 0.25$, $\alpha = 1$, $dt = 0.002$ s. Number of control points was equal to 30. A point source is located in the center of the model, $X_S = 4500$ m, $Y_S = 3500$ m, $Z_S = 100$ m.

Here, we want to exploit the high-frequency asymptotic properties of "fat" rays. In that case, we must achieve the best match between "fat" rays and standard rays, as we mentioned above. A software implementation of anisotropic ray tracing from the well-known package Madagaskar is used to calculate standard rays [22]. Figure 4a shows a 3D view of 50 rays calculated for a fixed azimuth angle $\varphi_{AZ} = -30deg$. and uniform dip angle increment of the wave front normal. In Fig. 4b projections of the rays on XY plane are demonstrated (top view). It can be seen that "fat" rays correspond closely with standard rays. Maximum deviations for ray trajectories for more than 5 km travel-paths do not exceed a few meters.

We have compared the so-called "travel-times" tables of the first arrivals of qP-waves calculated using "fat" and standard rays. To produce the tables, a set of 400×400 rays is constructed (the number of rays that have varying azimuth and dip angles) with takeoff angles lying in the intervals $\varphi_{AZ} = [0, 360^0]$, $\varphi_{Dip} = [0, 360^0]$. Next, the first arrivals travel times computed along each ray are interpolated to the regular grid using the approach described in [14]. As can be seen, the table is completely filled, which means there are no shadow areas (see Fig. 5a). The travel-time residuals between "fat" rays and standard rays do not exceed 3 ms. (Fig. 5b).

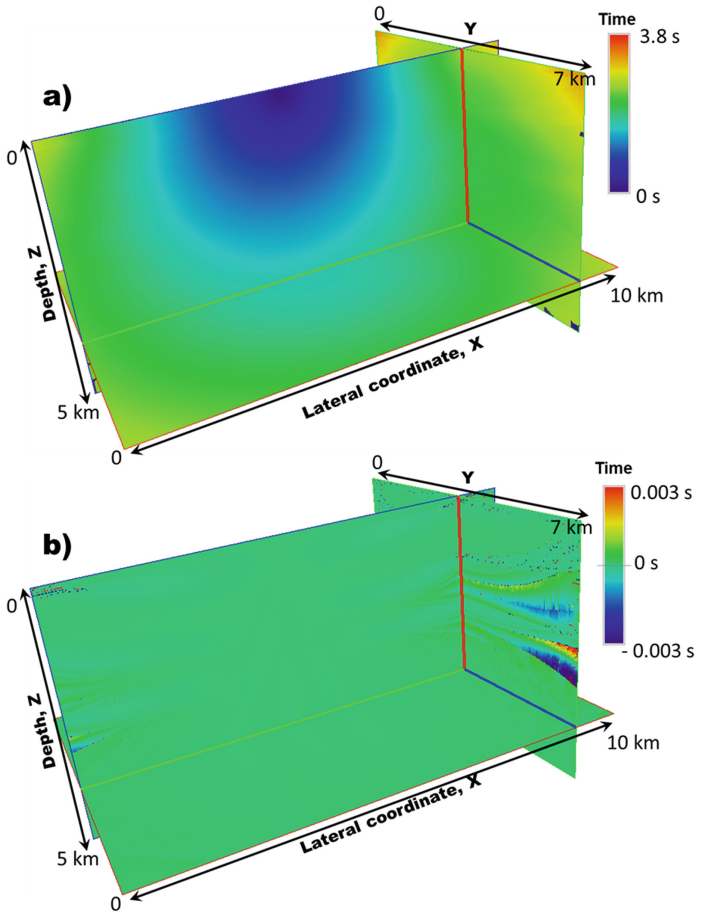


Fig. 5. a) First arrival travel-time table of the qP-wave calculated using the three-dimensional VTI model presented in Fig. 3 and "fat" rays with $\upsilon = 30$ Hz; b) First arrival travel-time residuals of the qP-wave calculated using "fat" rays with $\upsilon = 30$ Hz and standard rays (Madagaskar package).

We emphasize once again that the primary objective of the numerical experiment discussed above is to validate the correctness of both the concept of "fat" ray calculation in TTI media and its numerical implementation. For this reason, the appropriate value of the parameter υ has been chosen and the best match between the results obtained by the algorithm presented here and the standard procedure was required.

It is anticipated that "fat" rays will be utilized in media that are more sophisticated than the model presented above. When dealing with complex models with sharp interfaces, classical rays may struggle to calculate adequate ray trajectories and first arrival times. As previously demonstrated in [14], "fat" rays, with properly selected parameters, can handle this task quite effectively. Hence, it is necessary to choose the parameter υ optimally. The following considerations must be taken into account when selecting the "ray frequency". To ensure reliable passage of rays through sharp inhomogeneities (such as salt bodies), it is necessary to decrease the value of υ. It's crucial that "fat" rays don't differ too much from standard rays, and in simple parts of the model they should be similar to them. To fulfill this requirement, it is necessary to increase the value of υ. The choice of parameter υ for each particular case is a compromise between these two requirements and should be done empirically.

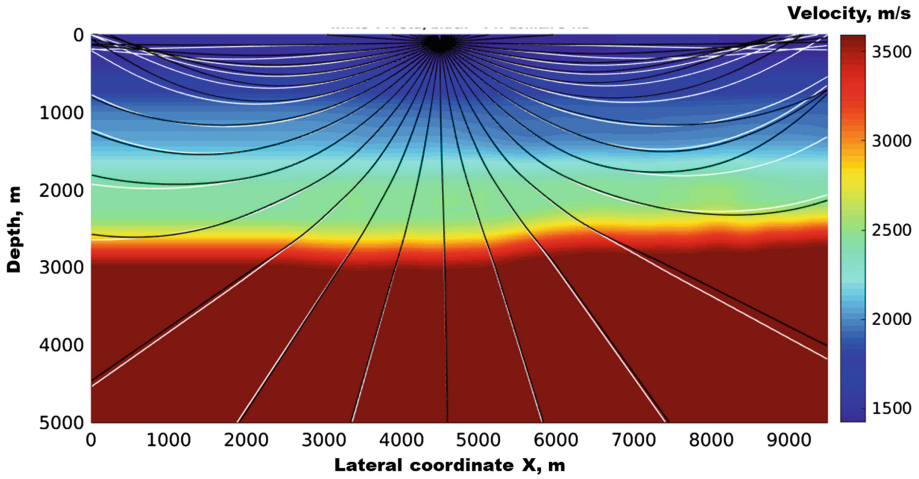


Fig. 6. Comparison of "fat" rays calculated for different frequencies. Rays for $\upsilon = 30$ Hz are shown in white (coincide with the standard rays), rays for $\upsilon = 5$ Hz are shown in black. Rays are calculated for a fixed azimuth $\varphi_{AZ} = 0$ and overlaid on 2D section of the phase velocity distribution.

Calculating "fat" rays takes much more computational time than standard rays for a given density of rays. One reason is that at each time step along the "fat" ray, multiple accesses to the velocity model are required to estimate the average phase velocity along the current front position. One more reason is that the number of control points chosen for ray tracing increases the computation time almost linearly. The number of control points should be sufficient to take into account the 3D velocity variation around a ray. If the number of control points is insufficient, it may cause instability of the ray. An

excessive number of control points leads to a significant increase in computational time without any noticeable improvement in the final result.

4.2 "Fat" Rays for Different Frequencies

Let's demonstrate numerically how frequency affects the behavior of "fat" rays. Figure 6 displays the calculated rays for two cases: $\upsilon = 30$ Hz and $\upsilon = 5$ Hz. The most significant difference can be seen in rays that have a propagation direction that is close to horizontal, particularly in the upper right part of the model. The obvious reason is that the model from Fig. 3 has the greatest variability in the vertical direction. In these conditions, 5 Hz "fat" rays are most sensitive to changes in the model parameters along the vertical axis.

4.3 Impact of Weak Anisotropy

It's interesting to assess the impact of weak anisotropy on the behavior of rays in the proposed model. The comparison of fat" rays at $\upsilon = 30$ Hz in isotropic and anisotropic cases can be seen in Fig. 7. To create an isotropic model from the VTI model from Fig. 3, we simply set the anisotropy parameters ε, δ to zero. The rays were derived for zero azimuth, that is, in the plane of (X, Z). It's evident that the behavior of the rays is significantly different. Once again, it confirms that even weak anisotropy can have a significant impact on the seismic data processing results.

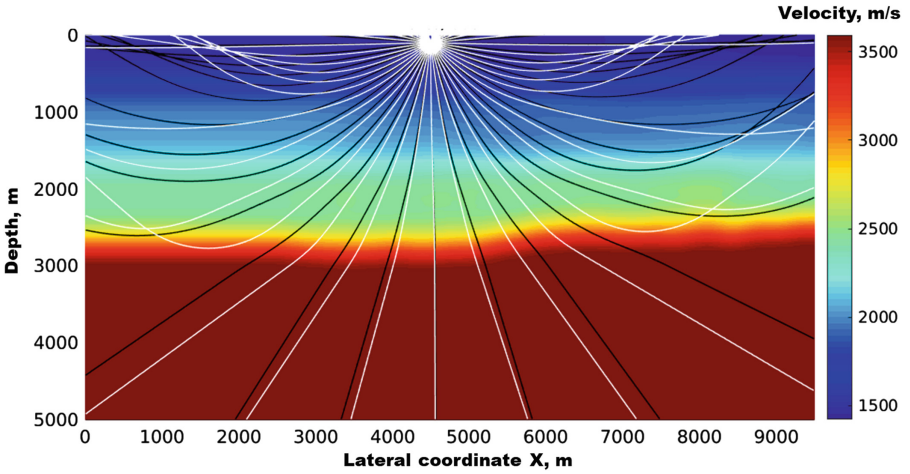


Fig. 7. Comparison of "fat" rays for $\upsilon = 30$ Hz in VTI model from Fig. 3 (shown in black) with the same rays in corresponding isotropic model ($\varepsilon = 0, \delta = 0$) (shown in white). Rays are calculated for a fixed azimuth $\varphi_{AZ} = 0$ and overlaid on 2D section of the phase velocity distribution.

In the general case of a TTI model with an arbitrary oriented symmetry axis, two additional arrays of parameters are required as input data. It is necessary to provide two volumes that provide symmetry axis orientation at every point in a model: a dip angle regarding the vertical axis, and azimuth.

4.4 qP-Waves Green's Function Calculation Using the Frequency Dependent Rays

In this chapter, we present numerical frequency domain elastic qP-wavefield simulation using the "fat" rays. The qP ray-based asymptotic Green's function in a weak anisotropic medium calculated at point R with the source at point S is defined as [20, 23, 24]:

$$G_{ij}(R,S) = \frac{g_j(S)g_i(R)}{4\pi\sqrt{\rho(S)\rho(R)V(S)V(R)}J(S,R)}\exp\{i\omega\tau(S,R)\} \tag{9}$$

where $g_j(S)$, $g_i(R)$ are components of polarization vector in the source and receiver points, V is phase velocity, ρ means density, $\tau(S,R)$ is traveltime between two points S and R. The symbol $J(S,R)$ means relative geometrical spreading along a ray. The geometrical spreading given by the expression:

$$J = \frac{dS}{d\Omega} \tag{10}$$

where dS is the elementary oriented surface of an orthogonal ray tube section at R and $d\Omega$ is the elementary solid angle associated with the ray tube at source. The finite-difference (FD) approximation of the geometrical spreading factor is calculated based on the theory provided in [2]. To utilize the FD approximation of geometrical spreading, one needs to consider a ray tube formed by three adjacent rays with small increments in take-off angles. In this case, it is important to have enough ray coverage in the target area. The amplitudes calculated along the ray tubes are interpolated into a regular grid. For ray-based wavefield simulation, we used a set of 500 x 500 rays. The parameters of ray tracing were as follows: $\upsilon = 5$ Hz, $l = 0.5$, $\theta_{max} = 0.5$, $\alpha = 1$. Density distribution was estimated using well known empirical Gardner equation [25]. In Fig. 10 we present three components of the frequency domain wavefield for frequency 5 Hz (real parts) calculated in the whole model. Vertical force was employed as the source at point S with coordinates $X_S = 4500$ m, $Y_S = 3500$ m, $Z_S = 100$ m. The solution error provided by "fat" rays in comparison with "exact" solution provided by exact 3D FD modelling does not exceed 9%.

All calculations presented above are done on a personal desktop computer with Intel Core i7-3770K 3.50 GHz CPU (4 core) and 32 Gb RAM. The "fat ray"-based Green function calculation for one source takes ~ 3.2 min of total computation time using all 4 CPU core. The most time-consuming part is ray tracing. It takes almost 80% of total time (Fig. 8).

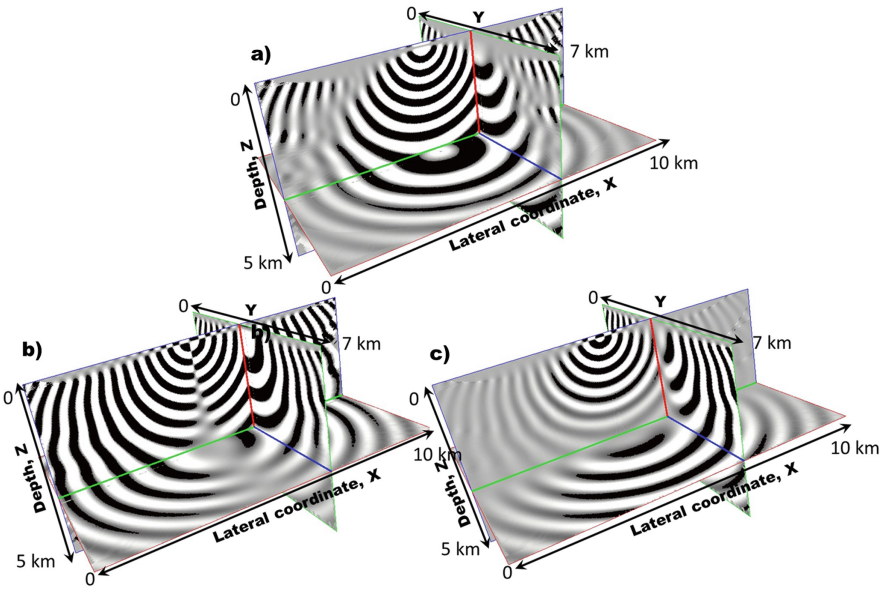


Fig. 8. qP-wave Green's function for frequency 5 Hz (real part) provided by the "fat" rays. a) Vertical (Z) component, b) Horizontal (X) component, c) Horizontal (Y) component. Vertical point force source was used.

5 Conclusions

In this work, an algorithm for constructing qP frequency-dependent rays ("fat" rays) in three-dimensional tilted transversely isotropic media with an arbitrary oriented axis of symmetry is developed, implemented and tested. The propagation of broadband seismic signals in real environments can be approximated using "fat" rays. The proposed scheme for calculating qP-"fat" rays consists of two stages. 1) Movement of the ray along the corresponding group velocity vector, which depends on the phase velocity smoothed along the flat element of the wave front and the current normal to the front. 2) Determination of the local orientation of the front at the ray point found in the first stage. The simultaneous movement of many control points, initially located on a fragment of a flat wave front in the vicinity of the ray, is used to find it. The motion of a locally flat fragment of the wave front is approximated in this manner. The distribution of model parameters in a specific volume of the medium concentrated around the ray is what determines the properties of "fat" rays. At each point, the wavelength determines the width of the sensitivity zone. To determine wavelength, a predefined parameter with frequency dimension is used, which is called the "ray frequency". In order to enhance numerical efficiency, approximate expressions for phase and group velocities for weak TTI media are employed. In most practical situations that arise in seismic exploration, this assumption is well-justified. To prove that the proposed concept is correct, a comparison was made between "fat" rays in the limiting case and standard rays using a smooth realistic model. In theory, both approaches should yield similar results in this situation. The accuracy of the proposed algorithm is confirmed by numerical results. Numerical experiments demonstrate that

"fat" rays can be quite successfully used to solve direct and inverse seismic problems in complex three-dimensional tilted transversely isotropic media.

Acknowledgments. The work is supported by RSF grant 21–71-20002. The numerical results of the work were obtained using computational resources of Peter the Great Saint-Petersburg Polytechnic University Supercomputing Centre (scc.spbstu.ru).

Disclosure of Interests. The authors have no competing interests to declare that are relevant to the content of this article.

References

1. Babich, V.M., Buldyrev, V.S.: Asymptotic Methods in Short-Wavelength Diffraction Theory. Alpha Science (2009)
2. Cerveny, V.: Seismic Ray Theory. Cambridge University Press, Cambridge (2001)
3. Kravtsov, Y.A., Orlov, Y.I.: Geometrical Optics of Inhomogeneous Media. Springer-Verlag, Heidelberg (1990)
4. Ben-Menahem, A., Beydoun, W.B.: Range of validity of seismic ray and beam methods in general inhomogeneous media – I. General theory. Geophys. J. Int. **82**, 207–234 (1985)
5. Williamson, P.: A guide to the limits of resolution imposed by scattering in ray tomography. Geophysics **56**, 202–207 (1991)
6. Marquering, H., Dahlen, F.A., Nolet, G.: Three-dimensional sensitivity kernels for finite-frequency traveltimes: the banana-doughnut paradox. Geophys. J. Int. **137**, 805–815 (1999)
7. Birch, A., Kosovichev, A.: Travel time sensitivity kernels. Solar Phys. **192**, 192–201 (2000)
8. Cerveny, V., Soares, J.E.P.: Fresnel volume ray tracing. Geophysics **57**, 902–915 (1992)
9. Lomax, A.: The wavelength-smoothing method for approximating broad-band wave propagation through complicated velocity structures. Geophys. J. Int. **117**, 313–334 (1994)
10. Vasco, D.W., Peterson, J.E., Majer, E.L.: Beyond ray tomography: wavepaths and Fresnel volumes. Geophysics **60**, 1790–1804 (1995)
11. Bube, K.P., Washbourne, J.K.: Wave tracing: ray tracing for the propagation of band-limited signals: part 1 – theory. Geophysics **73**, VE377–VE384 (2008)
12. Yarman, C.E., Cheng, X., Osypov, K., Nichols, D., Protasov, M.: Band-limited ray tracing. Geophys. Prosp. **61**, 1194–1205 (2013)
13. Vasco, D.W., Nihei, K.: Broad-band trajectory mechanics. Geophys. J. Int. **216**, 745–759 (2019)
14. Neklyudov, D., Protasov, M.: "Fat" rays in three dimensional media to approximate a broad-band signal propagation. In: Gervasi, O., et al. Computational Science and Its Applications – ICCSA 2023. LNCS, vol. 13957. Springer, Cham (2023). https://doi.org/10.1007/978-3-031-36808-0_8
15. Thomsen, L.: Weak elastic anisotropy. Geophysics **51**, 1954–1966 (1986)
16. Fowler, P.: Practical VTI approximations: a systematic anatomy. J. Appl. Geophys. **54**(3–4), 347–367 (2003)
17. Farra, V., Pšenčík, I.: Weak-anisotropy approximations of P-wave phase and ray velocities for anisotropy of arbitrary symmetry. Stud. Geophys. Geod. **60**, 403–418 (2016)
18. Grechka, V.: Applications of Seismic Anisotropy in the Oil and Gas Industry. EAGE (2009)

19. Farra, V.: High order expressions of the phase velocity and polarization of qP and qS waves in anisotropic media. Geophys. J. Int. **147**, 93–105 (2001)
20. Dehghan, K., Farra, V., Nicolétis, L.: Approximate ray tracing for qP-waves in inhomogeneous layered media with weak structural anisotropy. Geophysics **72**, SM47–SM60 (2007)
21. Woodward, V., Nichols, D., Zdraveva, O., Whitfield, P., Johns, T.: A decade of tomography. Geophysics **73**, VE5–VE11 (2008)
22. Madagaskar homepage. https://www.reproducibility.org/RSF/
23. Pšenčík, I.: Green's functions for inhomogeneous weakly anisotropic media. Geophys. J. Int. **135**, 279–288 (1998)
24. Pšenčík, I., Farra, V.: First-order P-wave ray synthetic seismograms in inhomogeneous weakly anisotropic media. Geophys. J. Int. **170**(3), 1243–1252 (2007)
25. Gardner, G., Gardner, L., Gregory, A.: Formation velocity and density – the diagnostic basics for stratigraphic traps. Geophysics **39**, 770–780 (1974)